

# Liver tumors segmentation from CTA images using voxels classification and affinity constraint propagation

Moti Freiman · Ofir Cooper · Dani Lischinski ·  
Leo Joskowicz

Received: 10 January 2010 / Accepted: 28 May 2010  
© CARS 2010

## Abstract

**Objective** We present a method and a validation study for the nearly automatic segmentation of liver tumors in CTA scans. **Materials and methods** Our method inputs a liver CTA scan and a small number of user-defined seeds. It first classifies the liver voxels into tumor and healthy tissue classes with an SVM classification engine from which a new set of high-quality seeds is generated. Next, an energy function describing the propagation of these seeds is defined over the 3D image. The functional consists of a set of linear equations that are optimized with the conjugate gradients method. The result is a continuous segmentation map that is thresholded to obtain a binary segmentation.

**Results** A retrospective study on a validated clinical dataset consisting of 20 tumors from nine patients' CTA scans from the MICCAI'08 3D Liver Tumors Segmentation Challenge Workshop yielded an average aggregate score of 67, an average symmetric surface distance of 1.76 mm (SD = 0.61 mm) which is better than the 2.0 mm of other methods on the same database, and a comparable volumetric overlap error (33.8 vs. 32.6%). The advantage of our method is that it requires less user interaction compared to other methods.

**Conclusion** Our results indicate that our method is accurate, efficient, and robust to wide variety of tumor types and is comparable or superior to other semi-automatic segmentation methods, with much less user interaction.

**Keywords** Liver tumors segmentation · Computed Tomography · Constraint optimization

## Introduction

Accurate detection and monitoring of liver tumors is a key task in many clinical applications. These include hepatomegaly and liver cirrhosis assessment, hepatic volumetry, hepatic transplantation planning, liver regeneration after hepatectomy, evaluation and planning for resection liver surgery, and monitoring of liver metastases, among many others. Repeatable and reliable detection and quantification of tumor burden and tumor volume is necessary for accurate and timely decision-making regarding therapy options.

Currently, most radiologists use simple guidelines to estimate tumor volume and response from clinical images. For 2D X-ray images, the 1979 World Health Organization [1] and the newer RECIST [2] guidelines define the tumor burden as the product of its maximum diameter—the largest distance between in-tumor points—and the maximum perpendicular diameter. This measure provides only a rough approximation from a single 2D projection image.

When 3D CTA images are available, radiologists estimate the tumor volume with the three-parameter ellipsoid formula:  $max-length \times max-depth \times max-width \times 0.5233$  [3]. This yields reasonable volume estimates for tumors with nearly spherical or ellipsoid shapes, which occur in specific types of benign and malignant tumors. However, it is less accurate for most other tumors, as they usually have irregular borders

---

Moti Freiman and Ofir Cooper are equally contributed.

---

M. Freiman (✉) · O. Cooper · D. Lischinski · L. Joskowicz  
School of Engineering and Computer Science,  
The Hebrew University of Jerusalem, Jerusalem, Israel  
e-mail: freiman@cs.huji.ac.il

O. Cooper  
e-mail: coopeo@cs.huji.ac.il

D. Lischinski  
e-mail: danix@cs.huji.ac.il

L. Joskowicz  
e-mail: josko@cs.huji.ac.il

and may have necrotic centers. An additional drawback of this method is that it quantifies the tumor shape with three dimensions, which limits its use in quantitative volumetric comparative studies.

Previous research shows that 3D volumetric measurements provide the best information for tumor progress monitoring [4–6]. The tumor volume can be measured by manual or semi-automatic tumors contours segmentation on multiple image slices. Volume calculation is then performed by incorporating the data obtained from each slice [7]. Manual and semi-automatic contouring, e.g. live wire segmentation [8], is time-consuming, user dependent, error prone, requires expert knowledge and produces variable results.

Liver tumor segmentation methods have the potential to provide fast, robust, user-independent accurate segmentations, and thus accurate and reliable tumor volume measures. Ideally, tumor segmentation should be automatic. However, when this is not feasible, nearly automatic segmentation, which requires little and intuitive interaction by a non-technical user, is an acceptable alternative for routine use in a clinical environment.

Automatic and nearly automatic CTA-based liver tumors segmentation is known to be a very challenging task. The main difficulties include the ambiguity of the liver and tumors boundaries, the complexity of the tumors surfaces, the contrast variability between the liver parenchyma, the liver vessels, and the tumors, the different tumor sizes and shapes, and the possible presence of many small metastases.

#### Previous work

In the past decade, researchers have developed a variety of methods for semi-automatic and automatic segmentation and visualization of liver structures. Most of these methods segment one structure at a time, usually starting with the liver surface, followed by the vessels and the tumors. The individual structure segmentation uses various techniques, such as intensity thresholding, region growing, and level-sets methods. One approach is to individually segment the liver surface, vessels, and tumors, and then perform a deformable model refinement for each [9,10]. Since this method does not use voxel neighborhood information, it may yield noisy or erroneous liver surface segmentations, especially when large tumors are present, as they bias the intensity distribution function. Metaxas et al. [11] use Markov random field (MRF) estimation coupled with deformable models for the segmentation of tumors. Peitgen et al. [12] describe an edge-based segmentation method for the liver contour and an interactive region-growing method for the vessels and tumors. Both methods require many seeds per CTA slice and are thus of limited clinical use.

Li et al. [13] use a machine learning technique to classify the one-dimensional intensity profiles of the liver tumors.

Since the method is biased to blob-like tumors, it is less accurate for tumors with irregular borders. Grady et al. [14] propose a random-walk-based 3D liver tumors segmentation based on a single user-defined seed. The additional seeds required by the random walker are generated from a 2D fuzzy-connectedness segmentation of the slice containing seed. Smeets et al. [15] couple spiral scanning with active contours-based propagation. These methods require at least one seed for each tumor, so they are not applicable for tumor detection and are impractical for livers with numerous metastases. In addition, Smeets et al. [15] require an additional interactive preprocessing step to cope with both hyper- and hypo-vascular tumors.

Liver tumor segmentation was the subject of a comprehensive dedicated workshop during the 2008 Medical Image Computing and Computer Aided Interventions (MICCAI) conference. The 3D Liver Tumors Segmentation Challenge (LTS08) Workshop Proceedings [16] includes 14 papers describing interactive, semi-automatic, and automatic liver tumors segmentation algorithms. The algorithms were tested on a database of 20 tumors from 9 clinical patient datasets from which ground-truth segmentations were manually generated by expert radiologists.

The interactive methods required extensive user interaction and yielded results whose accuracy is limited. For example, the best interactive method yields a mean The Volumetric Overlap Error (VOE) error of about 30%. Most of the semi-automatic methods used level-sets equations, whose solution required an initial contour around each individual tumor. While this initialization is relatively easier and faster for the user than that of the interactive methods, it is still not appropriate for routine clinical use. The automatic methods did not require any user interaction but had limited accuracy. We presented a nearly automatic method in which only a couple of seeds are required to initialize the segmentation algorithm [17,18]. This user interaction is appropriate for routine clinical use but yielded results with limited accuracy.

#### Contribution

In this paper, we present a new nearly automatic algorithm for the segmentation of liver tumors in computed tomography angiography (CTA) scans. The method requires only a small number of seeds—at least one for the liver and for each type of tumor—inside and outside the tumors. The seeds are used to classify the image voxels with a support vector machine (SVM) classification engine [19] from which a new set of high-quality seeds is generated. An energy function describing the propagation of the classified voxels is defined over the entire 3D image as a set of linear equations and is then efficiently solved with an iterative solver.

The main novelties of our method are as follows: (1) a method for selecting voxel seeds that are with high

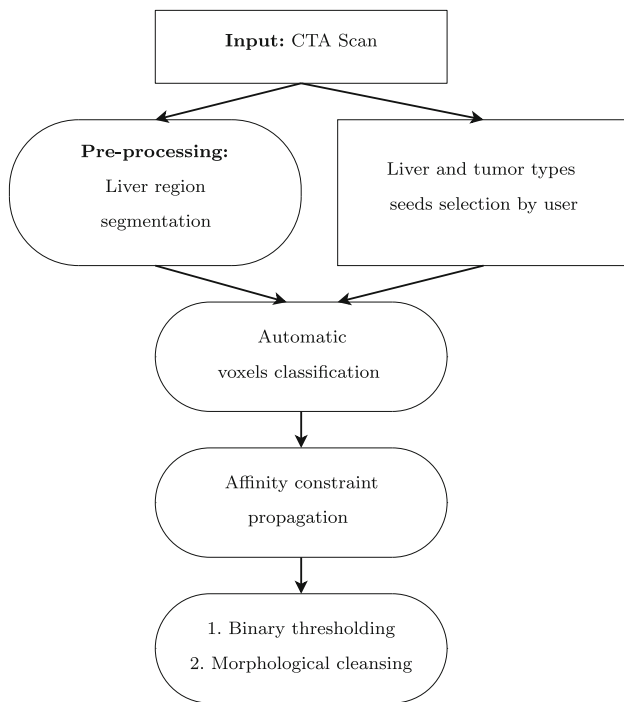


**Fig. 1** The flowchart of our method

probability inside the tumors and the liver parenchyma based on a statistical model build from a few user-defined seeds; (2) the extension of the affinity constraint optimization framework [20] from 2D to 3D and from using binary seeds only to handling fuzzy seeds, and; (3) the integration into an accurate nearly automatic liver tumors segmentation algorithm.

The experimental evaluation of our algorithm on the LTS08 database yielded an overall score of 67, which is comparable to the interactive algorithms results on this database, with much less user interaction. These results indicate that our algorithm produces accurate results for a wide variety of tumor types and may be practical in clinical use.

## Method

Our method is consists of four main steps:

1. Pre-processing: Liver region segmentation and tumor type seeds selection
2. Automatic voxels classification
3. Affinity constraint propagation
4. Binary thresholding and morphological cleansing

Figure 1 shows the flowchart of our method. We describe each step in detail next.

### Pre-processing

First, the entire liver region is segmented from the CTA image using a combination of intensity profiles analysis and morphological operators [21]. Next, the user interactively selects a few seeds in the liver parenchyma (background) and in the tumors (foreground) on the CTA slices. Unlike other semi-automatic methods [16], it suffices to have a few sample tumor seeds—at least one for each type of tumor, e.g., hyper-vascular or hypo-vascular tumors, regardless of their locations (Fig. 2a).

### Automatic voxels classification

The input to this phase is the liver region image  $I$  and the user-defined voxels  $S$ . A patient-specific statistical model describing the tumors and the liver classes is built using the support vector machine (SVM) classification engine [19]. The SVM is trained using the given user seeds  $S$ .

The training and classification stages proceed as follows. For each predefined voxel seed, we construct a feature vector consisting of four values: the mean, the standard deviation, and the minimum and the maximum intensity values in the  $5 \times 5 \times 5$  neighborhood of the voxel. The neighborhood statistics were selected experimentally as our features since they performed best when compared to other options such as the voxel value itself, and the voxel neighborhood gradients and Laplacian. The neighborhood size was determined by experimentation.

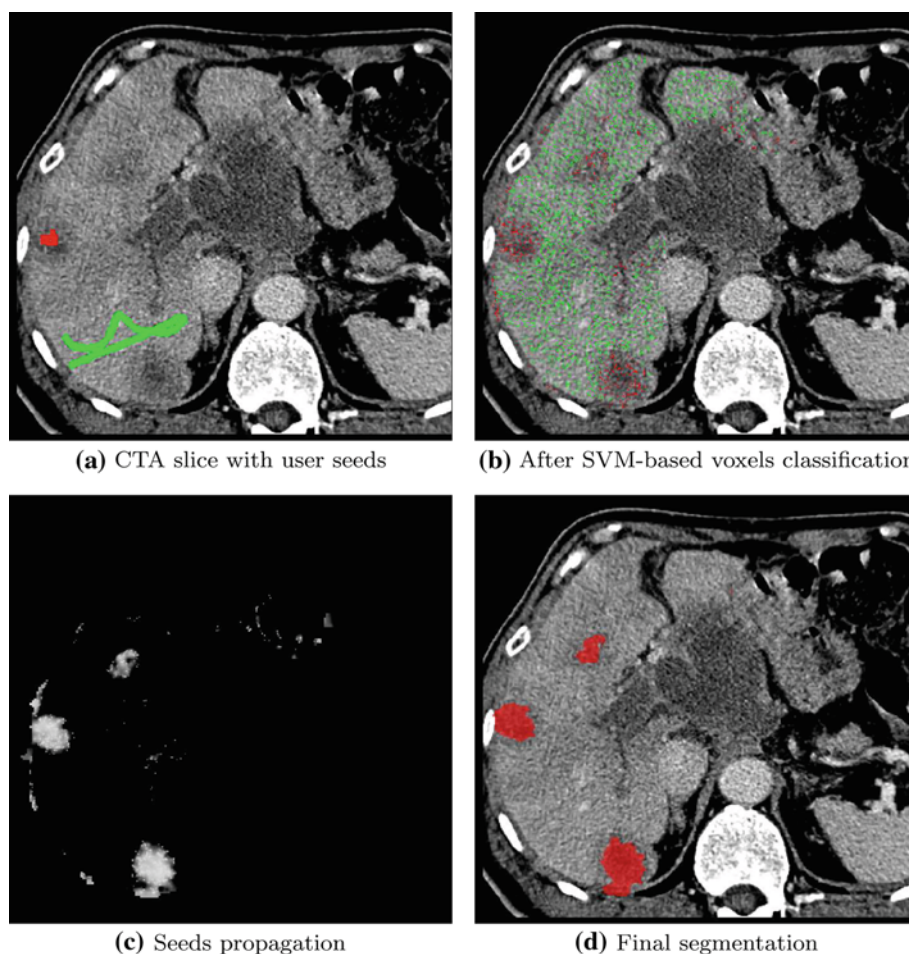
The SVM classification engine is then trained with these feature vectors. To separate the voxels that belong to the tumor class from those that belong to healthy tissues, we use a radial basis function as the kernel function. We then classify the rest of the voxels in the tumor according to this model. The SVM classification produced two fuzzy maps that represent the probability of each voxel to belong to the liver and to the tumor classes. To ensure high-quality seeds, we select only a small number by randomly sampling a portion (10–25%) of the image voxels and selecting those with a confidence level above 90%. Figure 2b shows the seeds that were selected by our method. Note that although the user marked only one tumor, our method was able to propagate this seed to the other tumors in the liver.

The resulting voxel classification by itself not sufficiently accurate for the tumor segmentation, as it does not take into account global information. such as the smoothness of the tumor surface. Therefore, additional processing is required.

### Affinity constraint propagation

The third step is to propagate the seeds obtained from the SVM classification to the entire image volume  $I$ . The propagation to neighboring voxels is based on the affinity between

**Fig. 2** Illustration of our liver tumors segmentation method: **a** background and tumor user-defined seeds (tumor seeds in *red* and healthy parenchyma in *green*); **b** result of the SVM-based voxels classification; **c** continuous propagation map, and; **d** binary segmentation after thresholding. Note that although the user marked only one tumor, our method generated tumor seed voxels for the other tumors as well



neighboring voxels. It is obtained by computing a global optimal propagation map of the seeds. The continuous segmentation map  $f$  of liver image  $I$  is defined as the minimum of an energy-like functional with two terms. The first is the data term that enforces conformance to the input seeds. The second is the smoothness term that ensures that the segmentation is as smooth as possible except across significant image edges. We formally define the energy function as:

$$f = \operatorname{argmin}_f \left( \sum_{\mathbf{x}} w(\mathbf{x})(f(\mathbf{x}) - g(\mathbf{x}))^2 + \lambda \sum_{\mathbf{x}} h(\nabla f, \nabla L) \right) \quad (1)$$

where  $g$  is the function of image  $I$ ,  $\mathbf{x}$  is the voxel index over  $I$ ,  $w$  is a binary indicator function that indicates if voxel  $\mathbf{x}$  is a seed voxel,  $\nabla$  is the gradient function,  $L$  is the logarithm of the original input image, and  $\lambda$  is a constant that controls the relative weight of the two terms in the functional.

The data term is designed to handle seeds with multiple labels and fractional confidence levels. It is defined as:

$$\sum_{c \in \text{labels}} \sum_{\mathbf{x}} w_c(\mathbf{x})(f(\mathbf{x}) - g_c(\mathbf{x}))^2 \quad (2)$$

where  $g_c$  and  $w_c$  are the classification and confidence maps for label type  $c$ , respectively [22].  $w_c \in [0, 1]$  and

$$\sum_c w_c(\mathbf{x}) = 1 \quad (3)$$

To segment the liver into healthy parenchyma and tumors, we define two labels, i.e., labels = {tumor, liver}. The introduction of the weights  $w_c$  allows the handling of fuzzy classified seed. This extends previously published method that handle only binary weights for the seeds [20].

The smoothness term  $h$  is defined as:

$$h(\nabla f, \nabla L) = \frac{|f_x|^2}{|L_x|^\alpha + \varepsilon} + \frac{|f_y|^2}{|L_y|^\alpha + \varepsilon} + \frac{|f_z|^2}{|L_z|^\alpha + \varepsilon} \quad (4)$$

where subscripts  $x$ ,  $y$ , and  $z$  denote the spatial differentiation of functions  $f$  and  $L$ , the exponent  $\alpha$  controls the sensitivity of the term to the derivatives of the log-input image, and  $\varepsilon$  is a small constant whose role is to avoid division by zero and to reduce the effect of image noise on  $h$  [20].

The resulting functional is expressed as set of linear equations using standard finite differences for the spatial derivatives of  $f$ . The quadratic expression in  $f$  has a unique global minimum that is obtained by solving the linear system:

$$Af = b$$

where

$$A_{ij} = \begin{cases} -\lambda (|L_i - L_j|^\alpha + \varepsilon)^{-1} & i, j \text{ are neighbors} \\ w_i - \sum_k A_{ik} & i = j \text{ and} \\ 0 & i, k \text{ are neighbors} \\ & \text{otherwise} \end{cases}$$

$$b(i) = \sum_{c \in \text{labels}} w_c(i) g_c(i) \quad (5)$$

where subscripts  $i$  and  $j$  denote image voxels, and  $c$  denotes a label number.

To obtain a unique solution, we solve the equation system once for each label type, in a one vs. all manner. When solving for label  $k$ , vector  $b$  is now defined as:

$$b(i) = w_k(i) g_k(i) - \sum_{c \in \text{labels} - \{k\}} w_c(i) g_c(i) \quad (6)$$

The matrix  $A$  is very large and would require more memory than is available in most computing environments. However, since  $A$  is a sparse, symmetric, and positive-definite matrix, iterative solvers can effectively solve this linear problem. We refer the reader to the Appendix for the proof that  $A$  is a symmetric, and positive-definite matrix.

The conjugate gradients algorithm with no preconditioner [23] efficiently solves the resulting equation system in near real time. Alternatively, a multi-grid approach such as those described by Lischinski et al. [20] or by Grady [24] can be used to speed up the computation.

### Binary thresholding and morphological cleansing

We compute a discrete segmentation from the resulting continuous segmentation map  $f$  for each label by direct thresholding. In our experiments, we use a constant threshold of 0.5 for the tumor class. To remove small isolated artifacts and small holes, we apply an erosion operator followed by a morphological region filling and hole filling [25].

## Experimental results

### Parameters analysis

The behavior of our algorithm depends mainly on three parameters: (1) the neighborhood size used for features extraction during the seeds classification; (2) the value of  $\lambda$ , which controls the weight of the smoothness term in our energy functional in Eq. 1, and; (3) the value of the exponent  $\alpha$ , which controls the sensitivity of the term to the derivatives of the log-input image in Eq. 4. To evaluate their impact on the algorithm performance, we run the algorithm on the training images of the 2008 MICCAI 3D Liver Tumors Segmentation

Challenge database (LTS08) [26] and set the algorithm parameters accordingly.

Figure 3 shows the results obtained using different parameters values. The neighborhood sizes were  $3 \times 3$ – $9 \times 9$ , the  $\lambda$  values varied from 1 to 3, and the  $\alpha$  values varied from  $10^{-7}$  to  $10^{-3}$ . Variations in the neighborhoods sizes from  $3 \times 3$  to  $9 \times 9$  yield inaccurate seeds classification, and therefore inaccurate segmentation. Small  $\alpha$  values cause the algorithm to be over sensitive to image gradients. Small  $\lambda$  values yield very conservative segmentation and may miss tumors borders altogether.

We found that the best values were  $\alpha = 10^{-5}$ ,  $\alpha = 2$ , and neighborhood size of  $5 \times 5$ .

### Tumors segmentation

We conducted a retrospective study on the LTS08 database [26]. This database consists of nine clinical CTA images with a total of 20 tumors from which ground-truth tumor segmentations were manually generated by expert radiologists. The datasets cover a wide range of patients and pathologies, including hepato-cellular carcinomas, hemangiomas, and metastases. The datasets were divided into two groups: The first group consists of 10 tumors from 4 CTAs and used for algorithm training and fine-tuning. The second group consists of 10 tumors from 5 CTAs and is used to evaluate the segmentation algorithms. To keep the objectiveness of the evaluation, the ground truth of the test datasets is not available to the users. The results are submitted to the database maintainer who evaluate their segmentation results and provides the relevant measurements and scores.

We compare our segmentation results with the ground truth with five metrics: (1) volumetric overlap error; (2) relative absolute volume difference; (3) average symmetric absolute surface distance; (4) symmetric RMS surface distance, and; (5) maximum symmetric absolute surface distance.

Table 1 summarizes the results. Our algorithm was able to detect tumors for which an initial seed was not provided. The best results were obtained for small tumors with strong edge gradients and for tumors surrounded by homogeneous liver tissue. Large tumors near the liver outer contour and tumors with weak gradients yielded lower scores. Tumors with a high gradient and a small amount of surrounding liver tissue yielded average scores.

We compared our results with those of the 14 methods in the MICCAI'08 workshop on the LTS08 database [16]. Our average symmetric surface distance of 1.76 mm (SD=0.61 mm) is better than the previously published result of 2.0 mm on the same database [15], while our volumetric overlap error is comparable with theirs (33.8 vs. 32.6%). The advantage of our method is that it does not require at least one seed for each tumor. Our average aggregate score of 67 is comparable to that of other

**Fig. 3** Parameters values evaluation: **a** CTA slice with ground-truth segmentation; **b** result obtained using different neighborhood size ( $3 \times 3$ – $9 \times 9$ ) for the seeds classification phase; **c** results obtained using different  $\alpha$  values ( $10e^{-3}$ – $10e^{-7}$ ), and; **d** results obtained using different  $\lambda$  values (1–3). The *blue contour* is the ground-truth segmentation, the *red contour* is the result with the lowest parameter value, and the *green contour* is the result with the highest parameter value

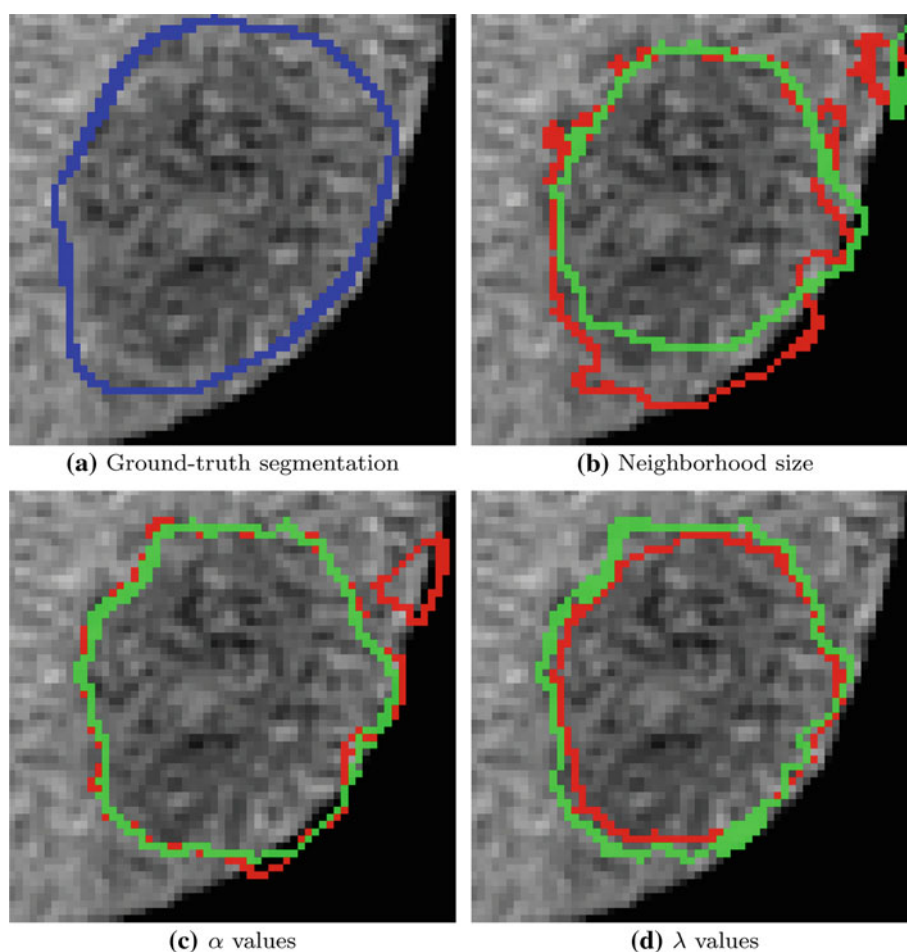


**Table 1** Comparison metrics and scores results

Dataset	Overlap error		Volume diff.		Avg. dist.		RMS dist.		Max. dist.		Total score
	(%)	Score	(%)	Score	(mm)	Score	(mm)	Score	(mm)	score	
IMG05_L1	28.19	78	23.90	75	2.01	49	2.95	59	12.00	70	66
IMG05_L2	37.72	71	5.42	94	1.39	66	1.79	75	6.33	84	78
IMG05_L3	36.72	72	21.51	78	1.54	70	2.27	68	9.26	77	71
IMG06_L1	61.45	53	56.57	41	1.89	79	2.27	68	5.75	86	60
IMG06_L2	43.01	67	37.91	61	1.04	42	1.45	80	6.21	84	73
IMG07_L1	17.68	86	5.89	94	2.63	33	4.59	36	37.06	7	51
IMG07_L2	27.61	79	12.28	87	1.56	77	2.89	60	22.78	43	66
IMG08_L1	21.38	83	11.75	88	2.32	54	3.26	55	20.85	48	63
IMG09_L1	48.33	63	37.35	61	2.44	83	3.64	49	11.84	70	56
IMG10_L1	15.95	88	13.78	86	0.79	69	1.13	84	5.25	87	85
Average	33.80	74	22.64	77	1.76	62	2.62	63	13.73	66	67

The first column indicates the dataset name. The following five columns show the measure and the score for each dataset. The last column shows the combined score. The bottom line shows the average for each measure

semi-automatic methods, with the advantage that our method requires much less user interaction. The mean computation time for each tumor was 8:35 mins (SD=5:13 mins) on an

PC with Intel Core2 Quad 2.4 GHz and 3GB of memory. The user time for the initial seeds selection was only a few seconds.

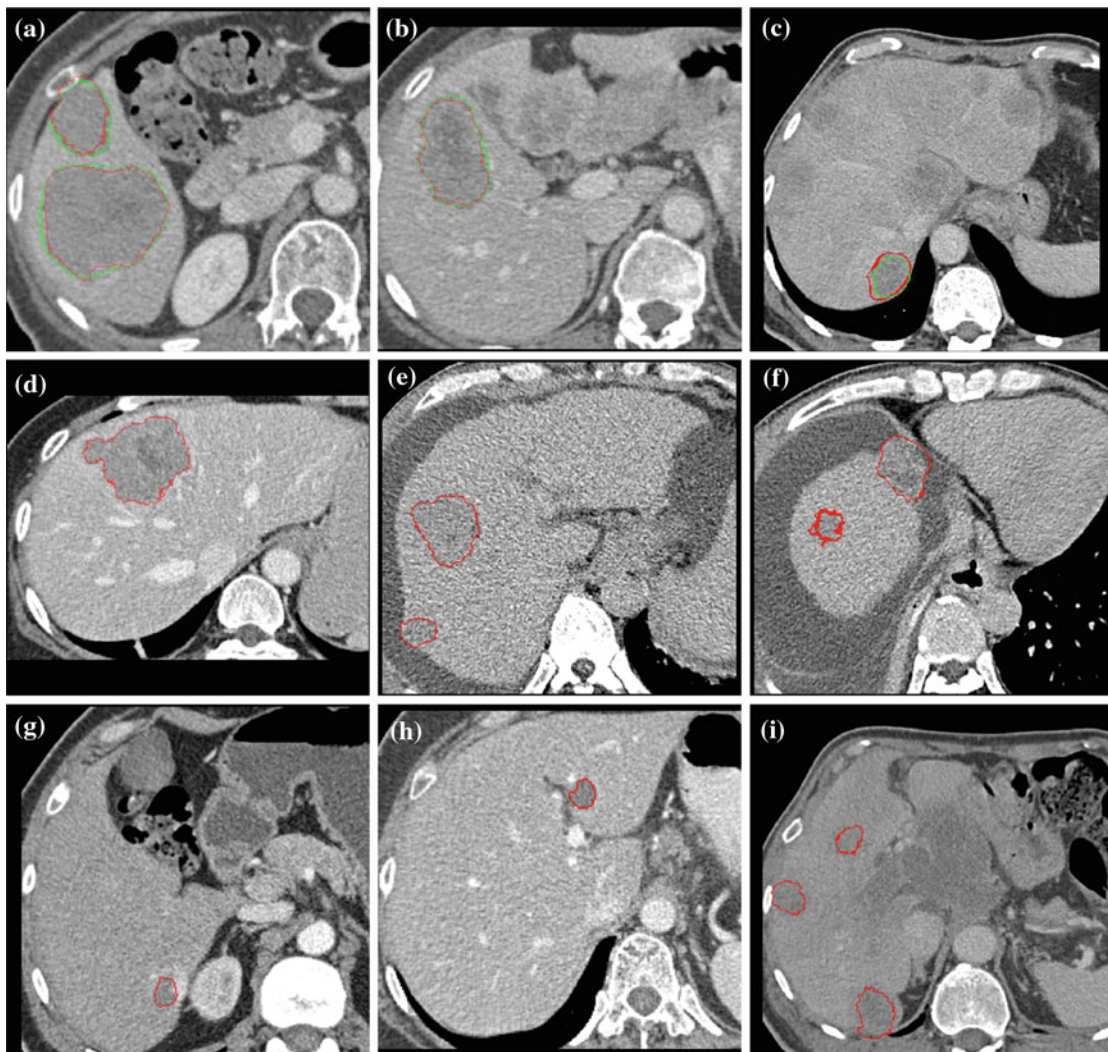


**Fig. 4** Liver tumors segmentation representative results: **a–c** results on the training datasets. The resulting segmentation contour (*red*) and the ground-truth contour (*green*) are overlaid on the original CTA image.

**d–i** Results on the test datasets. The resulting segmentation contour (*red*) is overlaid on the original CTA image

Figure 4 shows representative results of our method. Unlike other semi-automatic methods, e.g. [15], our method does not assume that the tissue surrounding the tumors is homogeneous, which makes our method more robust to different tumors locations.

## Conclusion

We have presented a new method and validation study for the nearly automatic segmentation of liver tumors. The tumor segmentation method described in this paper includes a novel method for voxel seeds selection that are with high probability inside the tumors and the liver parenchyma based on a statistical model build from a few user-defined seeds. The seeds are then used in an extended affinity constraint optimi-

zation framework that incorporates multiple labels with fractional confidence levels. The main advantages of our method are that it yields accurate results for a wide variety of tumor types with easy and fast user interaction. It does not require the identification of all tumors, as a few sample tumor seeds (at least one seed for each tumor type), regardless of their locations, are sufficient for the initialization. Our experimental results on the LTS08 database [26] show that our method is accurate, efficient, and robust when compared to manually generated ground-truth segmentation. It has a comparable or better performance than existing semi-automatic methods with substantially less user interaction.

Integrating nearly automatic methods into the daily clinical setup is expected to define new standards for volumetric liver tumor quantification. It will enable a better understanding of individual tumor natural history, help define the

treatment timing, and help improve the evaluation of therapy response. We are currently developing an integrated software package for the visualization and quantitative analysis of the liver to support diagnosis and surgical planning.

**Acknowledgments** This research is supported in part by MAGNETON grant 38652 from the Israeli Ministry of Trade and Industry. Moti Freiman is partially supported by the Hebrew University Hoffman Leadership and Responsibility Fellowship Program.

## Appendix

We prove in this Appendix that the matrix  $A$  is positive definite. Let  $W$  and  $K$  be two matrices such that  $A = W + K$ , where  $W = \text{diag}(w_1, w_2, \dots, w_n)$  is a diagonal matrix with diagonal vector  $w$ , and  $K$  is a non-homogeneous Laplacian matrix.

Consider now the quadratic expression  $x^T Ax$ . To prove that  $A$  is positive definite, we show that  $\forall x \neq 0, x^T Ax > 0$ . We decompose this term into two parts:

$$x^T Ax = x^T (W + K)x = x^T Wx + x^T Kx > 0 \quad (7)$$

We examine each term individually next. Let  $i$  and  $j$  be image voxels, and let  $i \sim j$  denote spatial proximity between voxels  $i$  and  $j$ . Then

$$x^T Wx = \sum_{i,j} x_i W_{ij} x_j = \sum_i w_i x_i^2 \geq 0 \quad (8)$$

The inequality holds because each term of the summation is non-negative. Similarly,

$$\begin{aligned} x^T Kx &= \sum_{i,j} x_i x_j K_{ij} = \sum_i x_i^2 K_{ii} + \sum_{i,j \sim i} x_i x_j K_{ij} \\ &= \sum_i \sum_{j \sim i} -x_i^2 K_{ij} + \sum_{i,j \sim i} x_i x_j K_{ij} \\ &= \sum_{i,j \sim i} -x_i^2 K_{ij} + x_i x_j K_{ij} \\ &= \sum_{i,j \sim i, j > i} x_i x_j K_{ij} + x_j x_i K_{ji} - x_i^2 K_{ij} - x_j^2 K_{ji} \\ &= \sum_{i,j \sim i, j > i} -K_{ij}(x_i^2 + x_j^2 - 2x_i x_j) \\ &= \sum_{i,j \sim i, j > i} -K_{ij}(x_i - x_j)^2 \geq 0 \end{aligned} \quad (9)$$

Once again, the inequality holds because each term of the summation is non-negative.

Now we claim that Eq. (7) holds because the terms in Eqs. (8), (9) cannot be simultaneously equal to zero. We prove this by contradiction. Assume that  $x^T Kx = 0$ . This implies that  $x_i = x_j$  for all voxels  $i, j$  which are neighbors. So  $x$  is a constant non-zero vector, as every voxel value equals that of its neighbors. In this case,  $x^T Wx > 0$  because there must be at least one  $w_i \neq 0$ . If all  $w_i$ 's are zero, this means

that no seed voxels have been chosen, which is not allowed. Thus,  $A$  is a positive-definite matrix.

## References

- World Health Organization, WHO handbook for reporting results of cancer treatment (1979)
- Eisenhauer E et al (2009) New response evaluation criteria in solid tumours: revised recist guideline (version 1.1). *Eur J Cancer* 45:228–247
- Goodwin S, Bonilla S, Sacks D, Reed R, Spies J, Landow W, Worthington-Kirsch R (2003) Reporting standards for uterine artery embolization for the treatment of uterine leiomyomata. *J Vasc Int Radiol* 14:467S–476S
- Tuma R (2006) Sometimes size does not matter: reevaluating recist and tumor response rate endpoints. *J Nat Cancer Inst* 98:1272–1274
- Tran L, Brown M, Goldin J, Yan X, Pais R, McNitt-Gray M, Gjertson D, Rogers S, Aberle D (2004) Comparison of treatment response classifications between unidimensional, bidimensional, and volumetric measurements of metastatic lung lesions on chest computed tomography. *Acad Radiol* 11:1355–1360
- Marten K, Auer F, Schmidt S, Kohl G, Rummeny E, Engelke C (2006) Inadequacy of manual measurements compared to automated CT volumetry in assessment of treatment response of pulmonary metastases using RECIST criteria. *Eur Radiol* 16:781–790
- Popa T, Ibanez L, Levy E, White A, Bruno J, Cleary K (2006) Tumor volume measurement and volume measurement comparison plug-ins for VolView using ITK. *SPIE Med Imaging* 6141:395–402
- Mortensen E, Barrett W (1998) Interactive segmentation with intelligent scissors. *Graph Models Image Process* 60:349–384
- Gao L, Heath D, Kuszyk B, Fishman E (1996) Automatic liver segmentation technique for 3D visualization of CT data. *Radiology* 201:359–364
- Soler L et al (2001) Fully automatic anatomical, pathological, and functional segmentation from CT scans for hepatic surgery. *Comp Aid Surg* 6:131–142
- Chen T, Metaxas D (2005) A hybrid framework for 3D medical image segmentation. *Med Image Anal* 9:547–565
- Bourquain H, Schenk A, Link F, Preim B, Prause G, Peitgen H (2002) Hepavision2a software assistant for preoperative planning in living related liver transplantation and oncologic liver surgery. In: *Proceedings of the 16th Conference on Computer Assisted Radiology and Surgery (CARS'02)*, pp 341–346
- Li Y, Hara S, Shimura K (2006) A machine learning approach for locating boundaries of liver tumors in ct images. In: *Proceedings of the 18th International Conference on Pattern Recognition (ICPR06)*, pp 400–403
- Jolly M-P, Grady L (2008) 3d general lesion segmentation in ct. In: *Proceedings of the 5th IEEE International Symposium on Biomedical Imaging (ISBI'08)*, IEEE, pp 796–799
- Smeets D, Loeckx D, Stijnen B, De Dobbelaer B, Vandermeulen D, Suetens P (2010) Semi-automatic level set segmentation of liver tumors combining a spiral-scanning technique with supervised fuzzy pixel classification. *Med Image Anal* 14:13–20
- Deng X, Du G (eds) (2008) *Proceedings of the 3D Segmentation in the Clinic: a Grand Challenge II—Liver Tumor Segmentation (LTS'08)*, <http://grand-challenge2008.bigrr.nl/proceedings/liver/articles.html>.
- Freiman M, Eliassaf O, Taieb Y, Joskowicz L, Sosna J (2008) A bayesian approach for liver analysis: algorithm and validation study. In: *Proceedings of the 11th International Conference of Medical Image Comp. and Computed Aided Intervention (MIC-CAI'08)*, vol. 5241 of LNCS, pp 85–92

18. Taieb Y, Eliassaf O, Freiman M, Joskowicz L, Sosna J (2008) An iterative bayesian approach for liver analysis: tumors validation study. In: Proceedings of the 3D Segmentation in the Clinic: A Grand Challenge II—Liver Tumor Segmentation (LTS'08)
19. Vapnik V (1995) The nature of statistical learning theory. Springer, New York
20. Lischinski D, Farbman Z, Uyttendaele M, Szeliski R (2006) Interactive local adjustment of tonal values. *ACM Trans Graph* 25:646–653
21. Freiman M, Eliassaf O, Taieb Y, Joskowicz L, Azraq Y, Sosna J (2008) An iterative bayesian approach for nearly automatic liver segmentation: algorithm and validation. *Int J Comput Assist Radiol Surgery (IJCARS)* 3:439–446
22. Li Y, Adelson E, Agarwala A (2008) ScribbleBoost: adding classification to edge-aware interpolation of local image and video adjustments. *Comp Graph Forum* 27:1255–1264
23. Saad Y (2003) Iterative methods for sparse linear systems. SIAM, 2nd edn
24. Grady L (2008) A lattice-preserving multigrid method for solving the inhomogeneous poisson equations used in image analysis. In: Proceedings of the 10th European Conference on Computer Vision, ECCV'2008, vol. 5303 of LNCS, Springer, pp 252–264
25. Ibanez L, Schroeder W, Ng L, Cates J (2005) The ITK Software Guide. Kitware, Inc. ISBN 1-930934-15-7, <http://www.itk.org/ItkSoftwareGuide.pdf>
26. <http://Its08.bigr.nl/>